Carbohydrate Polymers 140 (2016) 43–50

Contents lists available at ScienceDirect

Carbohydrate Polymers

journal homepage: www.elsevier.com/locate/carbpol

Flexible conductive nanocellulose combined with silicon nanoparticles and polyaniline

Minsung Park[a,1], Dajung Lee[a,1], Sungchul Shin[a], Hyun-Joong Kim[b], Jinho Hyun[a,c,*]

[a] Department of Biosystems and Biomaterials Science and Engineering, Seoul National University, Seoul 151-921, Republic of Korea
[b] Laboratory of Adhesion & Bio-Composites, Program in Environmental Materials Science, Seoul National University, Seoul 151-921, Republic of Korea
[c] Research Institute of Agriculture and Life Sciences, Seoul National University, Republic of Korea

ARTICLE INFO

Article history:
Received 11 September 2015
Received in revised form
17 December 2015
Accepted 21 December 2015
Available online 23 December 2015

Keywords:
Nanocellulose
Silicon nanoparticles
Polyaniline
Nanocomposites
Flexibility
Conductivity

ABSTRACT

Here we describe a unique conductive bacterial cellulose (BC) composite with silicon nanoparticles (SiNPs) and polyaniline. BC was used as a template for binding SiNPs resulting in a very promising anode material for Li-ion rechargeable batteries that showed a high specific capacity. The surfaces of the SiNPs were modified with phytic acid to enhance the binding of aniline monomer to the surface. A conformal coating of polyaniline (PANi) was formed on the modified SiNPs by *in situ* polymerization of aniline monomers. We also found that the phytic acid on the SiNPs was critical to ensure encapsulation of SiNPs with PANi. In addition, the phosphoric acid-tagged surface of the SiNPs enhanced the adhesion of SiNPs to the BC fibers. The resulting three dimensional network of BC was flexible and provided stress dissipation in the conductive BC composites. Flexural testing of conductive BC composites showed stable electrical conductivity even after repetitive bending over 100 times.

1. Introduction

The purpose of the investigation is the introduction of silicon nanoparticles (SiNPs) to bacterial cellulose (BC) having a unique three-dimensional networked structure and the conformal coating of polyaniline (PANi) to the SiNPs-bound BC composites. Since it is hard to polymerize aniline monomers at the surface of SiNPs, the surface of the SiNPs needs to be modified to enhance the binding of aniline monomers to the surface.

Rechargeable lithium ion batteries (LIBs) are one of the most promising systems for energy storage (Armand & Tarascon, 2008; Winter, Besenhard, Spahr, & Novak, 1998). Due to increasing demand for LIBs with low cost, high energy density and long cycle life, the development of new materials with high performance is required (Whittingham, 2004; Wu et al., 2012). The energy density of LIBs is able to be improved by replacing the graphitic carbonaceous anode with advanced anode materials which yield much higher capacities.

Silicon is a very promising anode material for Li-ion rechargeable batteries because its specific capacity is higher than that of graphite (Chiang, 2010; Wu & Cui, 2012; Zhang, 2011). However, silicon has poor conductivity and exhibits significant volume expansion upon Li-ion insertion, and these properties have restricted its application in anode materials (Ge, Rong, Fang, & Zhou, 2012; Kasavajjula, Wang, & Appleby, 2007). Recently, major efforts have been undertaken to address the conductivity problems of SiNPs using conducting polymers (Cui, Yang, Hsu, & Cui, 2009; Liu, Soares, Checkles, Zhao, & Yu, 2013; Liu et al., 2012). PANi is a popular option for increasing the conductivity of anode materials because it is chemically stable, lightweight and easy to synthesize. However, PANi is brittle and therefore cannot be used in applications like flexible batteries (Bhadra, Khastgir, Singha, & Lee, 2009; Genies, Boyle, Lapkowski, & Tsintavis, 1990). The fracture of electrodes can be prevented by introducing a flexible supporting matrix, which can dissipate stresses around the structure. A three-dimensionally networked fibrous structure can provide both flexibility and stress dissipation. BC biosynthesized by *Gluconacetobacter xylinus* can be a good supporting matrix for flexible conductive composites because of its unique 3D-networked structure and high mechanical and flexible properties (Chen, Huang, Liang, Guan, & Yu, 2013; Chen, Huang, Liang, Yao, et al., 2013; Siro & Plackett, 2010).

Several methods for the preparation of conductive cellulose have been reported. Carbonization of BC increased the

* Corresponding author at: Department of Biosystems and Biomaterials Science and Engineering, Seoul National University, Seoul 151-921, Republic of Korea.
E-mail address: jhyun@snu.ac.kr (J. Hyun).
[1] These authors contributed equally to this work.

http://dx.doi.org/10.1016/j.carbpol.2015.12.046
0144-8617/

conductivity significantly, but it could not maintain the mechanical property of cellulose due to the severe chain cleavage and loss of hydrogen bonding between the chains (Chen, Huang, Liang, Guan, et al., 2013; Wang et al., 2013). As a result, it was too brittle to handle and the application for the flexible devices could be restricted without incorporating with flexible elastomeric materials (Liang et al., 2012). The introduction of carbon nanotubes (CNTs) to BC was simple and effective for the increase of conductivity of cellulose (Choi, Park, Cheng, Park, & Hyun, 2012; Yoon, Jin, Kook, & Pyun, 2006). However, it was difficult to obtain the uniform conductivity due to the rapid aggregation and the localization of entangled CNTs.

The conformal coating of cellulose nanofibers with PANi is an important issue in conductive BC nanocomposites. Coating non-conductive cellulose fibers with PANi minimizes the loss of the conductivity compared with the simple incorporation of conductive nanoparticles such as CNTs. In spite of the effective coating on the cellulose nanofibers, the adsorption of aniline monomers is critical for the conformal coating of PANi at the surface of SiNPs. In this paper, phytic acid, which has six phosphoric acid groups, is introduced to the SiNPs to enhance the reaction with aniline monomers. the electrical stability of the conductive BC embedded with SiNPs when subjected to bending stress.

2. Experimental

2.1. Biosynthesis and purification of BC

G. xylinus (KCCM 40216) was obtained from the Korean Culture Center of Microorganisms. The bacterium was cultured on a mannitol medium composed of 2.5% (w/w) mannitol, 0.5% (w/w) yeast extract, and 0.3% (w/w) bacto-peptone. Bacteria were introduced into petri dishes containing culture medium at 28 °C for 5 days. After incubation, the BC membrane, which was biosynthesized on the surface of the liquid culture medium, was harvested and purified with 1 wt% NaOH (SAMCHUN Chemical, Korea) followed by washing with distilled water. The membrane was stored in distilled water prior to use.

2.2. Preparation of the silicon nanoparticle-embedded BC (Si-BC) composite

Forty milligrams of SiNPs (APS ≈ 100 nm, Alfa Aesar, USA) were dispersed in 100 mL deionized water by ultrasonicating for 3 min. Subsequently, 200 μL phytic acid (Sigma–Aldrich, USA) was added and the mixture was vigorously agitated using a magnetic stirrer for 1 h at room temperature. Then, SiNPs modified with phytic acid were collected by centrifugation at 1000 rpm and re-dispersed in 100 mL of deionized water. BC pellicles were cut into 4 cm × 4 cm square pieces, which were then immersed in the SiNPs dispersion solution for 1 day with stirring. The Si-BC composite was washed with deionized water and stored in water for further experiments. The immersion time of BC pellicles in the SiNPs dispersion solution was optimized by comparing the weight increase of Si-BC as shown in Supplementary Information (Fig. S1). The amount of SiNPs bound to the BC pellicles was calculated by the difference of weight between the BC and Si-BC dried at 60 °C for 1 day.

2.3. PANi polymerization with BC (PANi-BC) and Si-BC composite (PANi-Si-BC)

Aniline (0.91 mL, Sigma–Aldrich, USA) was added to 50 mL of a 0.5 N HCl solution containing BC and Si-BC composites. Then, the solution was stirred for 1 h to disperse the aniline monomers in the BC membranes. Subsequently, 2.28 g of ammonium persulfate (Duksan pure chemical, APS, Korea), was added to the solution as an oxidant to initiate the polymerization. The polymerization of aniline was carried out at 20 °C for 1 h. After polymerization, the composites were purified using methanol, distilled water and a 0.1 N HCl solution. The optimal conditions of polymerization were obtained by varying the molar ratio of APS to aniline monomer, the reaction temperature and the reaction time at the constant HCl concentration (Figs. S2–S4). The amount of PANi polymerized with Si-BC was calculated by the difference of weight between the Si-BC and PANi-Si-BC dried at 60 °C for 1 day. The samples were dried in a vacuum oven or in a freeze dryer prior to characterization of the composites.

2.4. Characterizations

The morphologies of the samples were observed using field emission scanning electron microscopy (FE-SEM, SUPRA 55VP, Carl Zeiss, Germany). The freeze-dried samples were cut into 1 cm × 1 cm sized pieces and were placed on conductive adhesive tape on aluminum stubs. To obtain the cross-sectional images of a BC hydrogel and SiNPs bound BCs, the samples were broken immediately after dipping in liquid nitrogen. The sample surfaces were coated with platinum using a sputter coater (SCD 005, BAL-TEC GmbH, Germany) before imaging. The imaging was performed in the "Inlens mode" at an acceleration voltage of 2 kV.

Electron transmission images of samples were captured by energy-filtering transmission electron microscopy (EF-TEM, LIBRA 120, Carl Zeiss, Germany). The Si-BC, PANi-BC, and PANi-Si-BC samples were immersed in separate vials with DI water and were ultrasonicated (VCX130, Sonic & Materials, USA) for 3 min at 40 W. Then, the solution with dispersed particles was dropped onto copper grids. The images were obtained at an acceleration voltage of 200 kV.

The crystal structure of the BC, phytic acid treated BC, Si-BC and PANi-Si-BC was determined using a high-resolution x-ray diffractometer (XRD, D8 DISCOVER, Bruker, Germany). For XRD experiments, 1 cm × 1 cm samples were cut from vacuum dried specimens. X-ray diffractometry (XRD) was performed using Cu Kα radiation.

Thermal degradation stability was measured by thermogravimetric analysis (TGA, TGA Q5000, TA Instruments, USA). About 10 mg of a vacuum dried sample was placed in an alumina crucible and was heated from room temperature to 600 °C at a heating rate of 10 °C min^{-1} under flowing nitrogen.

The electrical conductivity of the composites after exposure to flexural stress was measured by bending the samples using a universal testing machine (UTM, GB/LRX Plus, Lloyd, UK). To perform this test, 4 cm × 1 cm vacuum dried specimens were loaded into the machine and were bent at a constant speed of 50 mm min^{-1} at room temperature and 20% relative humidity. A 3 cm × 1 cm piece of aluminum foil was bonded to each end of the sample using silver paste (ELCOAT P-100, CANS, Korea) to allow connection of a digital multimeter (Chekman, Tae Kwang Electronics, Korea) for measuring the electrical conductivity. The bending radius of the samples was calculated as suggested in the literature (Wu et al., 2014). Specifically, the radius of the curvature (bending radius) was calculated as follows:

$$R = (d^2 + 4h^2)/8h$$

Here, d and h are the diameter and height of a dome, respectively. The change in electrical conductivity of the composites was measured after 100 repetitive bending cycles.

The percentage change in resistance was calculated as follows:

$$\Delta R(\%) = \{(R_0 - R_n)/R_n\} \times 100$$

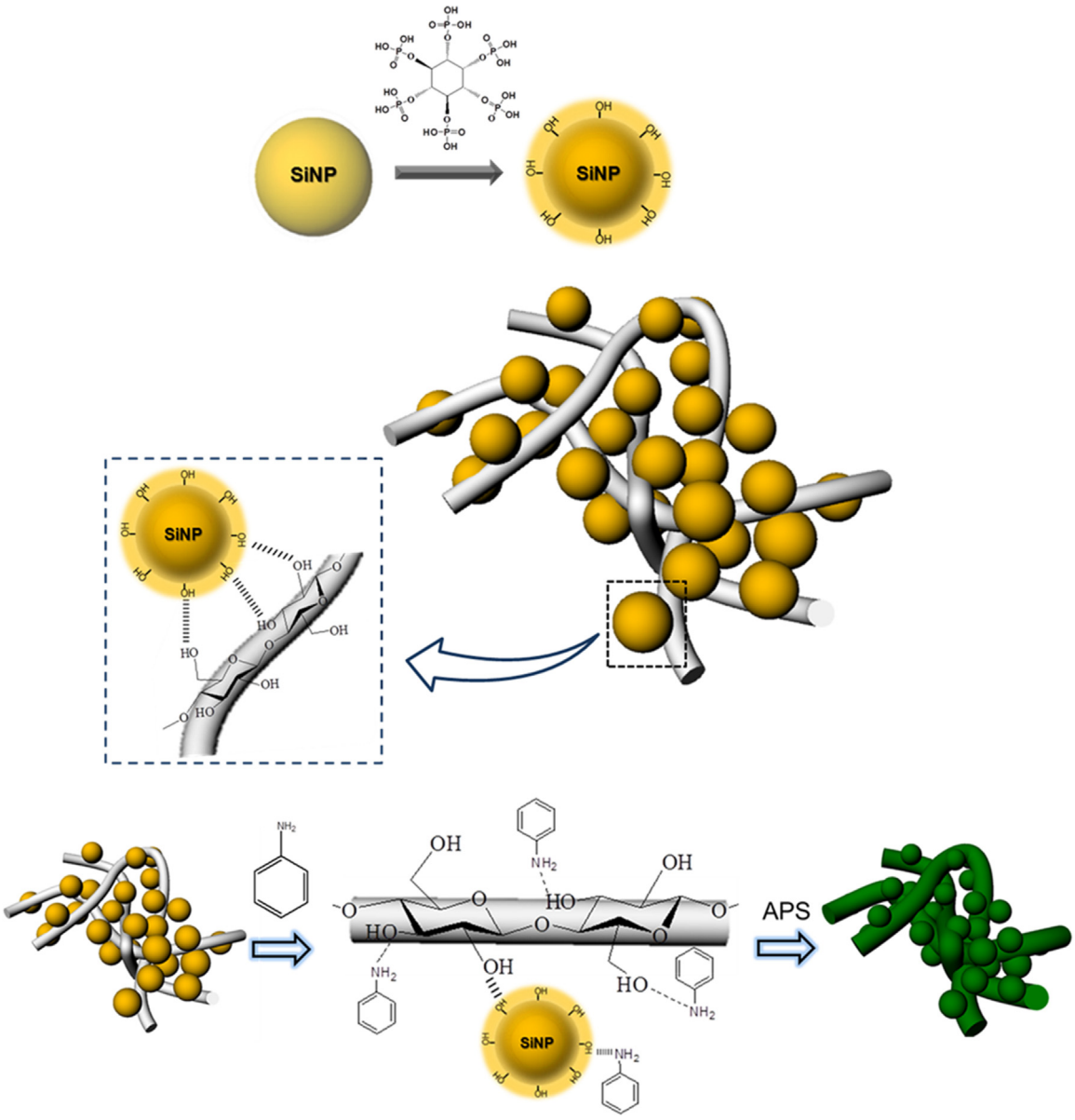

Scheme 1. Schematic representation of the process for preparing PANi-Si-BC composite. Hydroxyl groups were introduced on the surface of SiNPs as a result of modification with phytic acid. Hydroxyl groups of SiNPs can form hydrogen bonds with BC nanofibers. After adding aniline monomer and APS, PANi was polymerized on both BC nanofibers and SiNPs. The BC structure can serve as the template for both the adsorption of SiNPs and the polymerization of PANi.

where R_0 is the electrical resistance of the pristine composite, and R_n is the electrical resistance of the composite after bending n times.

3. Results and discussion

The adsorption of phytic acid on the SiNP surfaces resulted in a phosphoric acid-tagged SiNP surface. This allowed for immobilization of SiNPs onto the BC fibers through hydrogen bonding between the phosphoric acids of SiNPs and hydroxyl groups in the cellulose nanofibers (Scheme 1). Fig. 1A and 1B shows optical images of the pure BC and a Si-BC composite. SiNPs were introduced into a BC hydrogel by immersing the biosynthesized BC hydrogel into a well dispersed SiNP solution containing phytic acid for 1 day. The initially translucent BC hydrogel became opaque and brown (Fig. 1) because of the adsorption of SiNPs into the BC nanofibers. Silicon dioxide formed on the surface of SiNPs can interact with the phosphoric acid groups of phytic acid via hydrogen bonding (Scheme 1) (Wu et al., 2013). Though the hydrogen bonding between silicon dioxide and phosphoric acid is weak, the six phosphoric acid groups on a single phytic acid provide stable interactions between the phytic acid and SiNPs (Wu et al., 2013). Oxygen atoms in silicon dioxide can act only as acceptors during hydrogen bonding, but SiNPs modified with phytic acid have numerous hydroxyl groups that can serve as hydrogen bonding acceptors and donors (Harmon, 1992). Therefore, more SiNPs were adsorbed on the BC nanofibers after the modification of SiNPs with phytic acid than pure SiNPs during preparation of Si-BC. FT-IR spectrum of Si-BC was compared with that of BC bound with pure SiNPs without phytic acid to confirm the increase of hydrogen bonding between SiNPs and cellulose fibers. Unfortunately, it was not possible to obtain the evidence for the increased hydrogen bonding because the signal to noise ratio from the SiNPs surfaces was very low.

BC had a unique 3D-networked nanofiber structure, wherein the fiber diameters were several tens of nanometers (Fig. 2A). Cross-sectional images of BC showed a multilayered structure of cellulose with a spacing of about 5 μm as shown in Fig. 2C. SiNPs were well

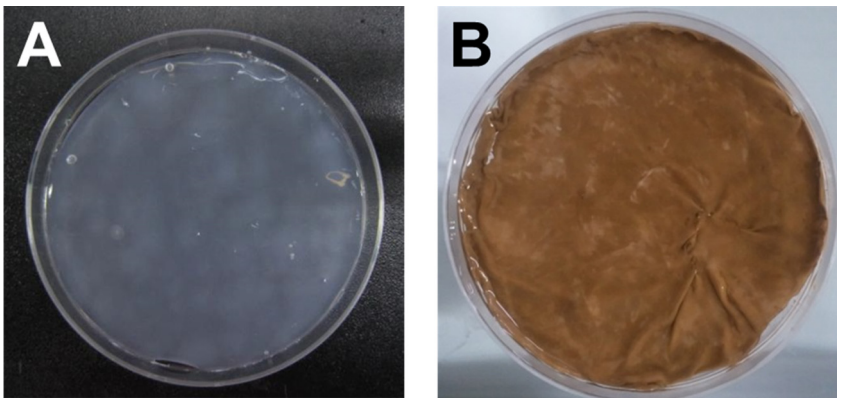

Fig. 1. Optical images of (A) pure BC and (B) Si-BC composite.

distributed over the BC membranes and were attached to the surface along the BC nanofibers without severe aggregation (Fig. 2B). We found SiNPs bound to the inner layer, the surface (through the relatively large pores), and the spacing between layers (Fig. 2D). Severe aggregation of SiNPs was not observed in the inner layers, and the space between the cellulose layers remained even after the attachment of SiNPs. The content of SiNPs in Si-BC was about 28.9% of the total weight by comparing the weights of BCs before and after SiNPs adsorption.

To impart conductivity to the Si-BC composite, PANi was polymerized at the nanofiber surface, which served as a template for PANi polymerization. First, Si-BC was dipped into the aniline solution. The aniline monomers permeated into the porous BC membranes, and amine groups on the aniline monomers formed hydrogen bonds with the hydroxyl groups of BC (Hu, Chen, Yang, Liu, & Wang, 2011) and the phosphoric acid groups of SiNPs coated with phytic acid (Wu et al., 2013). After adding an oxidant solution of APS, PANi polymerized on both the BC nanofibers and SiNPs (Scheme 1).

Compared with PANi on BC nanofibers alone (PANi-BC), PANi polymerized on Si-BC (PANi-Si-BC) had thicker granular structures along the fibers (Fig. 3). The typical spherical structure of SiNPs was not observed in PANi-Si-BC, but the surface of SiNPs was coated with PANi, which formed a porous, granular structure (Fig. 3B). The porous structure of PANi at the SiNPs enhanced the Li-ion diffusion and electrolyte penetration into the electrode, and provided free space for volume expansion of the SiNPs during electrochemical cycling when the material is used in Li-ion batteries. As shown in the cross-sectional image of PANi-Si-BC, aniline monomers diffused inside of the BC pellicles and polymerized to form highly porous PANi, which filled the spaces in the BC pellicles (Fig. 3C).

SiNPs coated with PANi were observed in the TEM images shown in Fig. 4. SiNPs were immobilized on the surface of the networked BC nanofibers, which showed reasonable stability after harsh ultrasonication (Fig. 4A). When aniline monomers were polymerized with unmodified SiNPs, PANi was not observed on the surface of the SiNPs. Instead, PANi with a branch-like morphology was formed in the bulk, as shown in Fig. 4B. SiNPs were encapsulated well by PANi when aniline monomers polymerized in the presence of phytic acid, (Fig. 4C). The increased affinity of SiNPs to PANi could be attributed to the hydrogen bonding between phosphoric acid groups of phytic acid at the SiNPs surface and amine groups of aniline monomers (Scheme 1). The gaps between the SiNPs in the Si-BC samples were

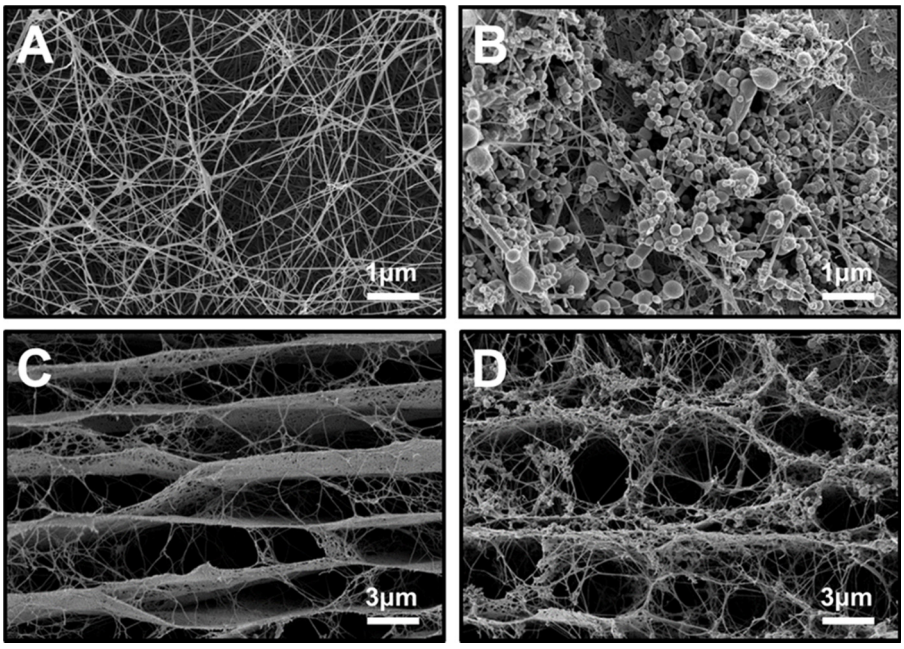

Fig. 2. FE-SEM images of BC and Si-BC composite. (A) Surface and (C) cross section of freeze-dried BC. (B) Surface and (D) cross section of freeze-dried Si-BC composite.

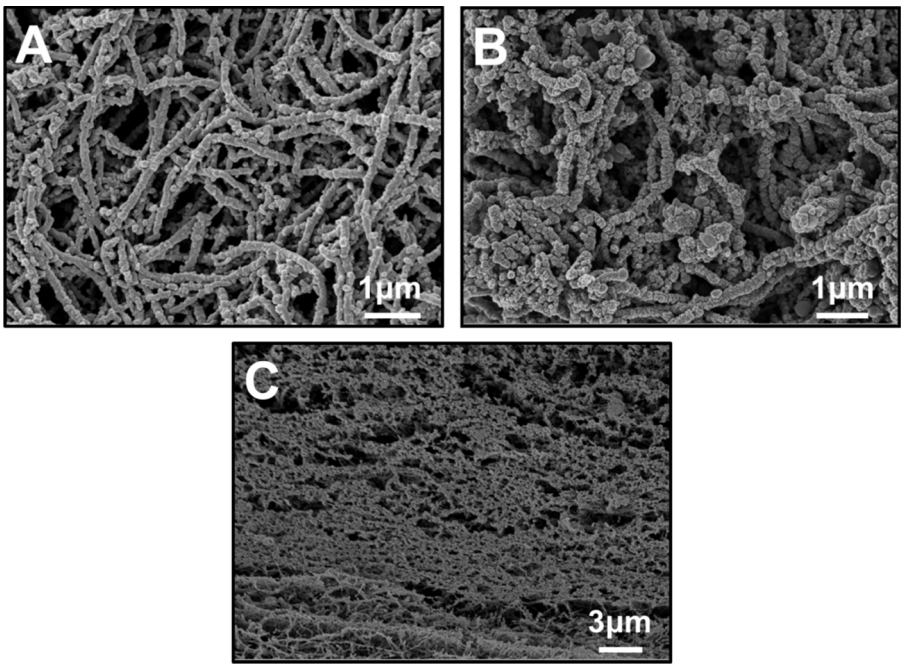

Fig. 3. SEM images of composites. (A) Surface image of PANi-BC, (B) surface image of Si-PANi BC, and (C) cross sectional images of freeze-dried PANi-Si-BC.

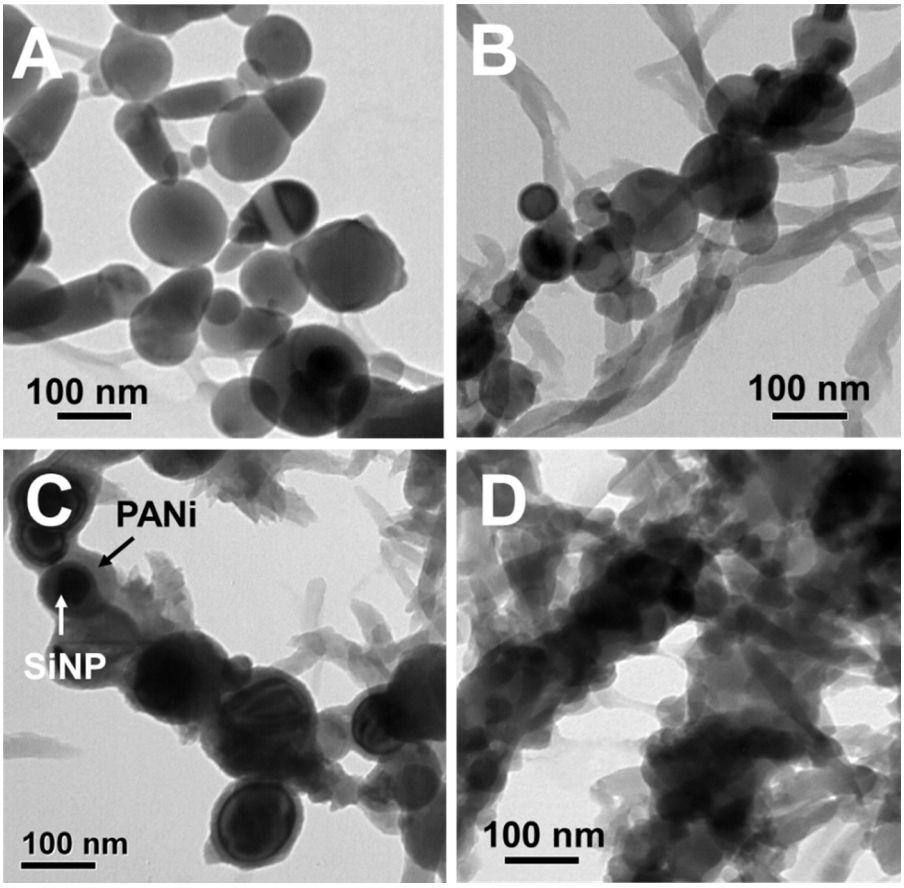

Fig. 4. TEM images of composites. (A) Si-BC and (B) Si-PANi without phytic acid. (C) Si-PANi and (D) PANi-Si-BC with phytic acid.

filled with PANi, which would provide the composite with better conductivity due to its compact structure (Fig. 4D).

The presence of SiNPs in the PANi-Si-BC composites was confirmed by XRD analysis (Fig. 5A). The XRD spectrum of the BC had two characteristic peaks at $2\theta = 14.6^\circ$, 22.6°, indexed to $(1\bar{1}0)$ and (200) reflections of cellulose I, respectively (Takai, Tsuta, Hayashi, & Watanabe, 1975). PANi-BC showed broad peaks at $2\theta = 14.7^\circ$, 20.3°, 25.2°, but the degree of crystallinity of the PANi was very low. The

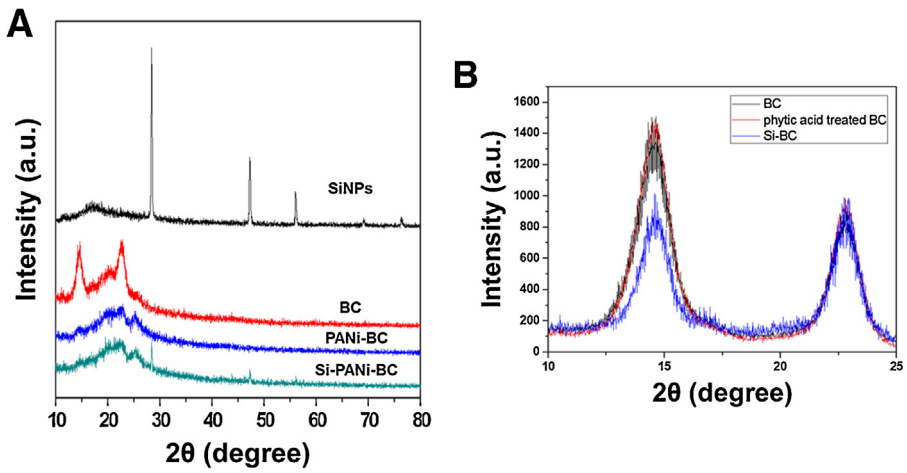

Fig. 5. XRD patterns of composites. (A) SiNPs, BC, PANi-BC, and PANi-Si-BC. (B) Change of crystallinity after the incorporation of SiNPs in BC.

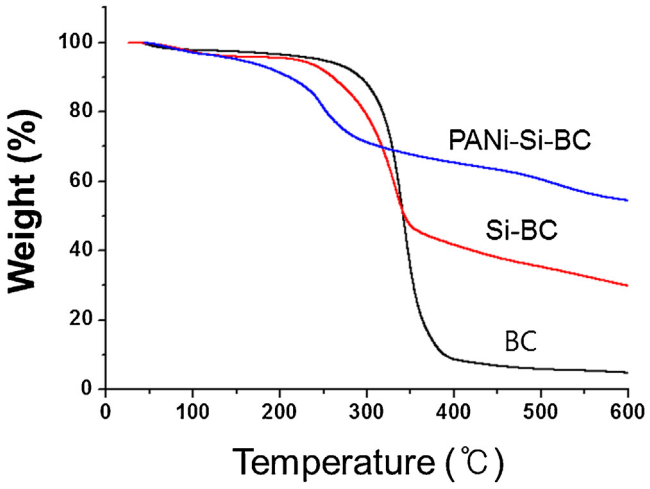

Fig. 6. Thermal stability of the composites. Thermogravimetric curves of BC, Si-BC and PANi-Si-BC were obtained using 10 mg of a vacuum dried sample in the range of temperature from 25 °C to 600 °C at a heating rate of 10 °C min^{-1} under flowing nitrogen.

two broad peaks at 20.3° and 25.2° were caused by the periodicity parallel and perpendicular to the polymer chain, respectively (Chaudhari & Kelkar, 1997; Lee, Kim, & Yang, 2012). The intensity of the BC peaks decreased as the amorphous PANi was synthesized on the BC nanofibers. PANi-Si-BC showed three additional peaks indexed to the (111), (200) and (311) planes of Si while PANi-BC without SiNPs did not show the assigned peaks for Si (Lee, Smith, Hayner, & Kung, 2010; Xu, Yin, Ma, Zuo, & Cheng, 2010). These observations confirmed that the SiNPs were well encapsulated in PANi on the BC composites. However, the presence of SiNPs in the composites reduced the ratio of the peak intensity at $2\theta = 14.6°$ to the peak intensity at $2\theta = 22.6°$ while the ratio of the peak intensities did not change for pure BC and phytic acid treated BC (Fig. 5B). It resulted from the restricted intermolecular interactions between the cellulose nanofibers whose space was occupied with ~100 nm size of SiNPs.

Fig. 6 shows TGA curves of the BC, Si-BC, and PANi-Si-BC. All samples showed a weight reduction of about 4% below 150 °C, which was attributed to water evaporation. The degradation of BC occurred at about 342 °C due to the cleavage of cellulose chains (Sureshkumar, Siswanto, & Lee, 2010). The residue of BC was 4.7% of the total weight at 600 °C. When normal BCs are dried, inter- and intramolecular hydrogen bonding occurs between the cellulose chains (Perotti, Barud, Ribeiro, & Constantino, 2014). In the case of Si-BC, the presence of SiNPs restricted the packing of cellulose chains during dehydration. For this reason, the first thermal degradation of Si-BC occurred at 331 °C, which was about 11 °C lower than the BC. However, the weight loss of Si-BC was smaller than BC due to the high thermal stability of SiNPs.

The weight residue of the Si-BC (initial weight percent SiNPs 28.9%, BC 71.1%) was 30.7% of the total weight at 600 °C (Fig. 6). Considering 4.7% of BC residue at 600 °C in the TGA curve, the weight residue of BC in Si-BC composite would be 3.3%. Therefore, the actual weight residue of SiNPs in the Si-BC composite was determined to be 27.4%. It was in agreement with 28.9% of the initial weight percent of SiNPs in the Si-BC composites.

The first degradation of PANi-Si-BC (initial weight percent PANi 63.5%, SiNPs 10.5%, BC 25.7%) occurred at 248 °C, which was much lower than normal BC or Si-BC. The degradation at lower temperature was associated to the weakened intermolecular hydrogen bonding of BC in the PANi-BC composite (Hu, Chen, Yang, Liu, & Wang, 2011), low molecular weight of polyaniline and dopant evaporates (Sinha, Bhadra, & Khastgir, 2009; Wei & Hsueh, 1989). The weight loss at 517 °C was attributed to the thermal degradation of polyaniline chains, and the weight residue of PANi-Si-BC was 54.4% at 600 °C (Chaudhari & Kelkar, 1997; Lee, Kim, & Yang, 2012).

The effect of phytic acid on the degradation of cellulose was investigated by the morphological change of the cellulose which was immersed in 0.2% phytic acid solution for 1 day (Fig. 7A). Since the phytic acid was used for the modification of SiNP surfaces rather than for the modification of cellulose fibers, the possibility of the direct degradation or catalytic degradation of cellulose chains would be negligible. XRD data did not show any significant difference between the BC and phytic acid treated BC confirming the chemical stability of BC. We also confirmed the thermal stability of BC immersed in phytic acid solution through the thermal decomposition behavior by TGA (Fig. 7B). The phytic acid treated BC showed a similar thermal decomposition behavior to normal BC and no significant difference could be found in the TGA curves.

Compared to the conductivity of other cellulose-based composite anodes such as graphite-microfibrillated cellulose (0.3 S/cm) (Jabbour et al., 2010, 2012) or polypyrrole–graphite–BC composites (0.1 S/cm) (Chen, Xu, Wang, Qian, & Sun, 2015), the PANi-Si-BC composite showed a smaller value of 0.017 S/cm due to the significant difference in conductivity between graphite and SiNPs (Fig. S4A).

Stable electrode conductivity is a critical factor because the brittleness of PANi is the main barrier to its use in flexible

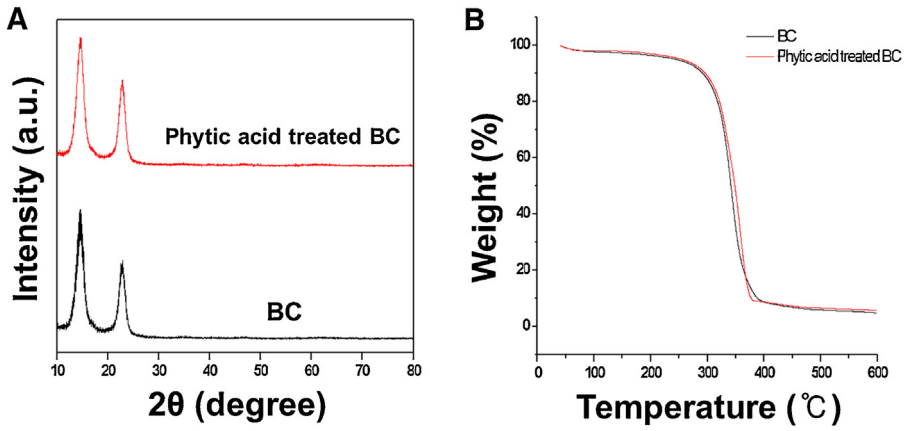

Fig. 7. Effect of phytic acid on the composites. (A) Morphological change and (B) the thermal stability of composites.

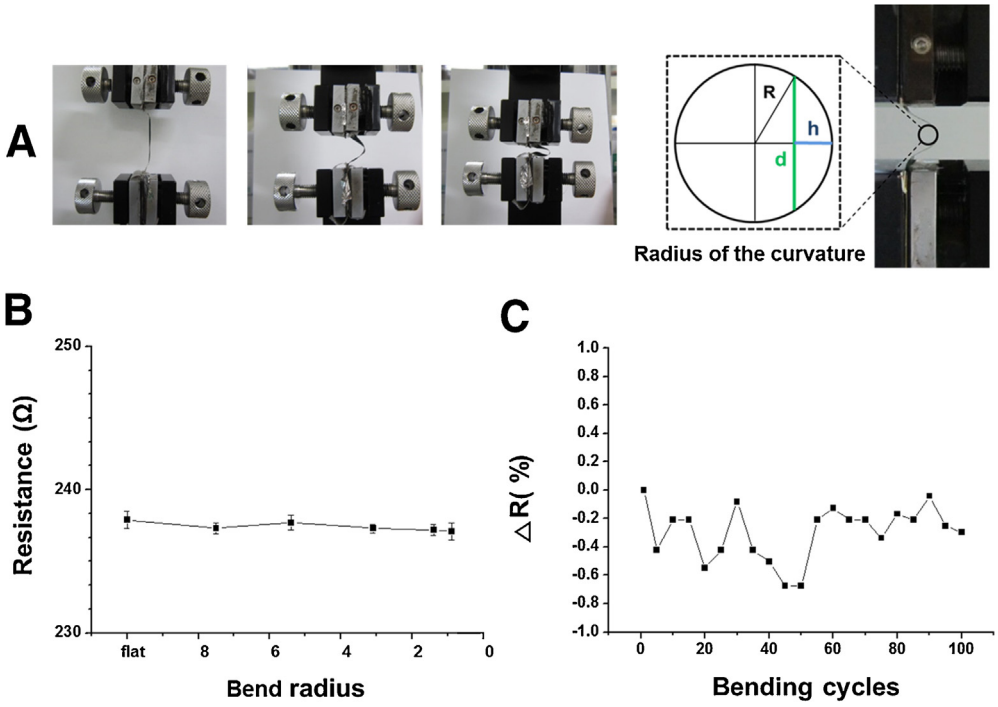

Fig. 8. Electrical stability of the composites to bending stress. (A) Optical images of bending process using UTM and parameters for the calculation of the bending radius, (B) resistance variation of PANi-Si-BC composite for changes in bending radius, and (C) the percentage of resistance change of the composite according to bending cycle up to 100 cycles.

batteries. Therefore, we investigated the conductivity of BC composites under bending stress. Prior to the conductivity measurement, we found out that the electrical properties of the composites could be changed by the moisture adsorption due to the sensitivity of cellulose to the moisture. First, samples were stored in desiccator until the use and the measurement of electrical conductivity was performed at 20% relative humidity and room temperature. PANi-Si-BC composites were bent while the conductivity was continuously measured. The radius of curvature was calculated based on a diagram of a dome formed during application of the bending stress (Fig. 8A). As shown in Fig. 8B, PANi-Si-BC composites did not show significant changes in resistance over the whole range of bending curvature. Based on these data, we concluded that BC provided mechanical stability to the composites by providing a characteristic 3D networked structure. Stable conductivity under repetitive bending stress is important for reliable electrical applications. PANi-Si-BC retained its initial conductivity for 100 bending stress cycles, which confirmed its reliability as a flexible electrical component (Fig. 8C).

4. Conclusions

BC was used both as a binding template for SiNPs and as a template for *in situ* polymerization of 3D networked PANi. SiNPs were uniformly attached to the surface of BC pellicles along the nanofibers. Phytic acid enhanced the binding efficiency of SiNPs to both BC nanofibers and aniline by providing increased hydrogen bonding. The conductive PANi-Si-BC composite showed stable conductivity under repetitive bending stresses, which confirmed its potential for use as a flexible anode component in flexible rechargeable batteries.

Acknowledgements

This research was supported by the Basic Science Research Program through the National Research Foundation of Korea (NRF), funded by the Ministry of Science, ICT & Future Planning (Grant Number 2014016093).

Appendix A. Supplementary data

Supplementary data associated with this article can be found, in the online version, at doi:10.1016/j.carbpol.2015.12.046.

References

Armand, M., & Tarascon, J. M. (2008). Building better batteries. *Nature*, *451*(7179), 652–657.
Bhadra, S., Khastgir, D., Singha, N. K., & Lee, J. H. (2009). Progress in preparation, processing and applications of polyaniline. *Progress in Polymer Science*, *34*(8), 783–810.
Chaudhari, H. K., & Kelkar, D. S. (1997). Investigation of structure and electrical conductivity in doped polyaniline. *Polymer International*, *42*(4), 380–384.
Chen, J. H., Xu, J. K., Wang, K., Qian, X. R., & Sun, R. C. (2015). Highly thermostable, flexible, and conductive films prepared from cellulose, graphite, and polypyrrole nanoparticles. *ACS Applied Materials & Interfaces*, *7*(28), 15641–15648.
Chen, L. F., Huang, Z. H., Liang, H. W., Guan, Q. F., & Yu, S. H. (2013). Bacterial-cellulose-derived carbon nanofiber@MnO_2 and nitrogen-doped carbon nanofiber electrode materials: An asymmetric supercapacitor with high energy and power density. *Advanced Materials*, *25*(34), 4746–4752.
Chen, L. F., Huang, Z. H., Liang, H. W., Yao, W. T., Yu, Z. Y., & Yu, S. H. (2013). Flexible all-solid-state high-power supercapacitor fabricated with nitrogen-doped carbon nanofiber electrode material derived from bacterial cellulose. *Energy & Environmental Science*, *6*(11), 3331–3338.
Chiang, Y. M. (2010). Building a better battery. *Science*, *330*(6010), 1485–1486.
Choi, J., Park, S., Cheng, J., Park, M., & Hyun, J. (2012). Amphiphilic comb-like polymer for harvest of conductive nano-cellulose. *Colloids and Surfaces B: Biointerfaces*, *89*, 161–166.
Cui, L. F., Yang, Y., Hsu, C. M., & Cui, Y. (2009). Carbon–silicon core–shell nanowires as high capacity electrode for lithium ion batteries. *Nano Letters*, *9*(9), 3370–3374.
Ge, M. Y., Rong, J. P., Fang, X., & Zhou, C. W. (2012). Porous doped silicon nanowires for lithium ion battery anode with long cycle life. *Nano Letters*, *12*(5), 2318–2323.
Genies, E. M., Boyle, A., Lapkowski, M., & Tsintavis, C. (1990). Polyaniline – A historical survey. *Synthetic Metals*, *36*(2), 139–182.
Harmon, K. M. (1992). Hydrogen-bonding in biological structures – Jeffrey, G.A., Saenger, W. *Science*, *257*(5077), 1774–1775.
Hu, W. L., Chen, S. Y., Yang, Z. H., Liu, L. T., & Wang, H. P. (2011). Flexible electrically conductive nanocomposite membrane based on bacterial cellulose and polyaniline. *Journal of Physical Chemistry B*, *115*(26), 8453–8457.
Jabbour, L., Destro, M., Gerbaldi, C., Chaussy, D., Penazzi, N., & Beneventi, D. (2012). Aqueous processing of cellulose based paper-anodes for flexible Li-ion batteries. *Journal of Materials Chemistry*, *22*(7), 3227–3233.
Jabbour, L., Gerbaldi, C., Chaussy, D., Zeno, E., Bodoardo, S., & Beneventi, D. (2010). Microfibrillated cellulose-graphite nanocomposites for highly flexible paper-like Li-ion battery electrodes. *Journal of Materials Chemistry*, *20*(35), 7344–7347.
Kasavajjula, U., Wang, C. S., & Appleby, A. J. (2007). Nano- and bulk-silicon-based insertion anodes for lithium-ion secondary cells. *Journal of Power Sources*, *163*(2), 1003–1039.
Lee, B. H., Kim, H. J., & Yang, H. S. (2012). Polymerization of aniline on bacterial cellulose and characterization of bacterial cellulose/polyaniline nanocomposite films. *Current Applied Physics*, *12*(1), 75–80.
Lee, J. K., Smith, K. B., Hayner, C. M., & Kung, H. H. (2010). Silicon nanoparticles-graphene paper composites for Li ion battery anodes. *Chemical Communications*, *46*(12), 2025–2027.
Liang, H. W., Guan, Q. F., Zhu-Zhu, Song, L. T., Yao, H. B., Lei, X., et al. (2012). Highly conductive and stretchable conductors fabricated from bacterial cellulose. *NPG Asia Materials*, 4.
Liu, B. R., Soares, P., Checkles, C., Zhao, Y., & Yu, G. H. (2013). Three-dimensional hierarchical ternary nanostructures for high-performance Li-ion battery anodes. *Nano Letters*, *13*(7), 3414–3419.
Liu, N., Wu, H., McDowell, M. T., Yao, Y., Wang, C. M., & Cui, Y. (2012). A yolk–shell design for stabilized and scalable Li-ion battery alloy anodes. *Nano Letters*, *12*(6), 3315–3321.
Perotti, G. F., Barud, H. S., Ribeiro, S. J. L., & Constantino, V. R. L. (2014). Bacterial cellulose as a template for preparation of hydrotalcite-like compounds. *Journal of the Brazilian Chemical Society*, *25*(9), 1647–1655.
Sinha, S., Bhadra, S., & Khastgir, D. (2009). Effect of dopant type on the properties of polyaniline. *Journal of Applied Polymer Science*, *112*(5), 3135–3140.
Siro, I., & Plackett, D. (2010). Microfibrillated cellulose and new nanocomposite materials: A review. *Cellulose*, *17*(3), 459–494.
Sureshkumar, M., Siswanto, D. Y., & Lee, C. K. (2010). Magnetic antimicrobial nanocomposite based on bacterial cellulose and silver nanoparticles. *Journal of Materials Chemistry*, *20*(33), 6948–6955.
Takai, M., Tsuta, Y., Hayashi, J., & Watanabe, S. (1975). Biosynthesis of cellulose by acetobacter-xylinum. 3. X-ray studies of preferential orientation of crystallites in a bacterial cellulose membrane. *Polymer Journal*, *7*(2), 157–164.
Wang, B., Li, X. L., Luo, B., Yang, J. X., Wang, X. J., Song, Q., et al. (2013). Pyrolyzed bacterial cellulose: A versatile support for lithium ion battery anode materials. *Small*, *9*(14), 2399–2404.
Wei, Y., & Hsueh, K. F. (1989). Thermal-analysis of chemically synthesized polyaniline and effects of thermal aging on conductivity. *Journal of Polymer Science Part A: Polymer Chemistry*, *27*(13), 4351–4363.
Whittingham, M. S. (2004). Lithium batteries and cathode materials. *Chemical Reviews*, *104*(10), 4271–4301.
Winter, M., Besenhard, J. O., Spahr, M. E., & Novak, P. (1998). Insertion electrode materials for rechargeable lithium batteries. *Advanced Materials*, *10*(10), 725–763.
Wu, H., Chan, G., Choi, J. W., Ryu, I., Yao, Y., McDowell, M. T., et al. (2012). Stable cycling of double-walled silicon nanotube battery anodes through solid–electrolyte interphase control. *Nature Nanotechnology*, *7*(5), 309–314.
Wu, H., & Cui, Y. (2012). Designing nanostructured Si anodes for high energy lithium ion batteries. *Nano Today*, *7*(5), 414–429.
Wu, H., Yu, G. H., Pan, L. J., Liu, N. A., McDowell, M. T., Bao, Z. A., et al. (2013). Stable Li-ion battery anodes by in-situ polymerization of conducting hydrogel to conformally coat silicon nanoparticles. *Nature Communications*, 4.
Wu, T. F., Yen, T. M., Han, Y. Y., Chiu, Y. J., Lin, E. Y. S., & Loa, Y. H. (2014). A light-sheet microscope compatible with mobile devices for label-free intracellular imaging and biosensing. *Lab on a Chip*, *14*(17), 3341–3348.
Xu, Y. H., Yin, G. P., Ma, Y. L., Zuo, P. J., & Cheng, X. Q. (2010). Nanosized core/shell silicon@carbon anode material for lithium ion batteries with polyvinylidene fluoride as carbon source. *Journal of Materials Chemistry*, *20*(16), 3216–3220.
Yoon, S. H., Jin, H. J., Kook, M. C., & Pyun, Y. R. (2006). Electrically conductive bacterial cellulose by incorporation of carbon nanotubes. *Biomacromolecules*, *7*(4), 1280–1284.
Zhang, W. J. (2011). A review of the electrochemical performance of alloy anodes for lithium-ion batteries. *Journal of Power Sources*, *196*(1), 13–24.